Dynamic Behavior of Caputo Fractional-Order Model of Forest Biomass, Human Population, and Atmospheric Carbon Dioxide

Moh. Nurul Huda[1,2], Agus Suryanto[1*], Isnani Darti[1], Muhammad Fakhruddin[3]

[1]Department of Mathematics, Faculty of Sciences, Brawijaya University, Malang 65145, Indonesia
[2]Department of Mathematics, Faculty of Sciences, Mulawarman University, Samarinda 75123, Indonesia
[3]Research Center for Computing, National Research and Innovation Agency (BRIN), Bogor 16911, Indonesia

[*]Email: suryanto@ub.ac.id

Abstract

This study aims to analyze the dynamical model of CO_2 concentration, human population, and forest biomass. Human activities and land-use changes in forested areas play an important role as the primary contributors to the increase in CO_2 emissions, which drive global warming. The inclusion of fractional-order derivatives is considered to examine the long-term memory effects on the interactions within the CO_2 concentration model. Theoretical results such as the existence, uniqueness, positivity, and boundedness of solutions, the local and global stability behavior of equilibrium points, and the existence of a Hopf bifurcation are explored. Furthermore, key parameters, including the deforestation rate and memory order, are investigated to determine their influence on the solution behavior of the CO_2 concentration model. A fractional-order numerical scheme is employed to illustrate various scenarios, validating the theoretical findings. The results show that fractional-order changes affect the dynamic behavior of the model. In addition, increased deforestation rates can increase CO_2 concentrations and reduce human population in the long term.

Keywords: Carbon dioxide, deforestation, forest biomass, global stability, Hopf bifurcation

2020 MSC classification number: 26A33, 34D23, 34C23, 92B05, 92D40

1. INTRODUCTION

Carbon dioxide (CO_2) is one of the principal greenhouse gases driving global warming [1]. Increasing atmospheric CO_2 concentrations trap heat that would otherwise escape into space, thereby intensifying the greenhouse effect [2]. Since the onset of the Industrial Revolution, CO_2 levels have risen from approximately 280 parts per million (ppm) in the 18th century to over 420 ppm in 2023 [3]. This accumulation enhances heat retention within the Earth's atmosphere, leading to rising global mean temperatures, accelerated polar ice melt, and shifts in extreme weather patterns, including more severe floods, droughts, and storms. Such impacts pose substantial risks to both natural ecosystems and human well-being, contributing to agricultural instability, malnutrition, and the spread of infectious diseases, including those transmitted by vectors [4, 5].

The escalation of atmospheric CO_2 concentrations is predominantly attributable to anthropogenic activities, notably the combustion of fossil fuels—coal, oil, and natural gas for energy production, transportation, and industrial processes [6]. These activities collectively release billions of tonnes of CO_2 into the atmosphere each year. Furthermore, deforestation and unsustainable land-use changes diminish the planet's natural capacity to absorb CO_2, as forests act as critical carbon sinks. Intensive agricultural practices, industrial waste emissions, and inadequate waste management further amplify greenhouse gas emissions, thereby accelerating the disruption of the natural carbon cycle. Effective mitigation strategies such as transitioning to renewable energy sources and implementing large-scale reforestation are therefore essential in addressing these challenges [7].

The dynamics of atmospheric CO_2 concentrations have been extensively investigated through applied mathematical modeling. Traditionally, such studies employ classical integer order nonlinear models. For example, Misra and Verma [8] developed a model describing changes in atmospheric CO_2 concentration, which was later extended by Misra and Jha [9, 10] to incorporate factors such as renewable energy adoption and economic growth. Tandon [11] examined the influence of industrial activities particularly mining on

[*]Corresponding Author
Received September 17^{th}, 2025, Revised October 23^{rd}, 2025, Accepted for publication February 2^{nd}, 2026.
Published by Indonesian Biomathematical Society, e-ISSN: 2549-2896, DOI:10.5614/cbms.2026.9.1.2

ecosystems, emphasizing how resource exploitation can disrupt the natural interactions between vegetation and CO_2. Similarly, Jha et al. [12] analyzed the effects of anthropogenic CO_2 emissions on wildlife populations, with subsequent work by Jha and Misra [13] exploring carbon taxation as a policy instrument for emission control.

A common limitation in these classical models is the neglect of non-local effects and memory properties, which are critical for accurately representing biological and environmental processes. Fractional-order derivatives offer a more realistic framework by capturing these long-term memory effects and non-local interactions. The intrinsic non-locality of fractional operators enables a more faithful representation of model dynamics compared to classical derivatives [14].

In recent years, the classical CO_2 dynamics model of Misra and Verma [8] has been reformulated using various fractional derivatives. For instance, Ilhan et al. [15] analyzed the model with the Caputo–Fabrizio (CF) fractional operator and developed a numerical scheme combining the Laplace transform with homotopy analysis methods. Dubey et al. [16] employed the Caputo operator within a hybrid homotopy analysis–Sumudu transform framework. Singh et al. [17] applied the Katugampola fractional operator and solved the system using a combination of q-homotopy analysis and generalized Laplace transforms. These studies primarily focused on advancing numerical schemes for solving the system proposed in [8], yet none have addressed the Caputo fractional operator in the context of a dynamic analysis of CO_2 concentration.

From the reviewed literature, no existing fractional-order mathematical model employing the Caputo operator has been reported to investigate the dynamic behavior of atmospheric CO_2 concentration. In this study, we extend the model of Misra and Verma (2013) [8] by formulating a Caputo-type fractional-order version, in which atmospheric CO_2 concentration, human population, and forest biomass are represented as interconnected compartments. The introduction of fractional-order derivatives allows for the incorporation of memory effects into the model, thereby enabling a more realistic analysis of long-term interactions, particularly in assessing the impact of deforestation on forest biomass.

2. THE MODEL FORMULATION

A model of atmospheric CO_2 concentration dynamics influenced by forest biomass and human population activity in a classical integer-order derivative framework was proposed by Misra and Verma [8]. In the classical setting, the rate of change of each state variable depends only on its current value and the present interactions with other variables, without accounting for any historical influence. This framework is expressed as

$$\begin{aligned}
\frac{dX}{dt} &= Q_0 + \lambda N - \alpha X - \lambda_1 XF, \\
\frac{dN}{dt} &= sN\left(1 - \frac{N}{L}\right) - \theta XN + \pi\varphi NF, \\
\frac{dF}{dt} &= uF\left(1 - \frac{F}{M}\right) - \varphi NF + \pi_1\lambda_1 XF.
\end{aligned} \tag{1}$$

where $X(t)$ denotes atmospheric CO_2 concentration, $N(t)$ the human population, and $F(t)$ the forest biomass.

The classical model (1) captures direct interactions effectively, but it does not incorporate memory effects—that is, the influence of past states on the current dynamics. In reality, many biological and environmental processes, including CO_2 dynamics, possess long-term memory and non-local effects. For example, the current CO_2 concentration depends on historical emissions and the cumulative impact of deforestation over extended periods.

We address this limitation by reformulating the classical model (1) into a fractional-order model that uses Caputo-type derivatives of order $q \in (0, 1)$. The fractional derivative includes an integral term over the model's history, which embeds memory effects and non-local interactions into the model. The fractional-order model is given by

$$\begin{aligned}
\frac{d^q X}{dt^q} &= Q_0 + \lambda N - \alpha X - \lambda_1 XF, \\
\frac{d^q N}{dt^q} &= sN\left(1 - \frac{N}{L}\right) - \theta XN + \pi\varphi NF, \\
\frac{d^q F}{dt^q} &= uF\left(1 - \frac{F}{M}\right) - \varphi NF + \pi_1\lambda_1 XF.
\end{aligned} \tag{2}$$

where $\frac{d^q}{dt^q}$ denotes the Caputo-type fractional derivative defined as

$$\frac{d^q f(t)}{dt^q} = \frac{1}{\Gamma(n-q)} \int_0^t \frac{f^{'}(\nu)}{(t-\nu)^{n-q-1}} d\nu, \tag{3}$$

where $\Gamma(\cdot)$ is the Gamma function and $q \in (0,1)$ [18]. In both systems, the parameters are identical and non-negative for $t \geq 0$, with their descriptions provided in Table 1. The classical model (1) assumes instantaneous response, whereas the fractional model (2) accounts for the influence of prior states on current dynamics, enabling a more realistic representation of processes such as the delayed impact of deforestation on CO_2 concentration and forest biomass recovery.

Table 1: Description of parameters in the model (2).

Symbol	Parameter description
Q_0	Natural increase rate of atmospheric CO_2
λ	Growth rate of atmospheric CO_2 caused by anthropogenic factors
α	Natural decrease rate of atmospheric CO_2
λ_1	Decrease rate of atmospheric CO_2 due to forest biomass
L	Carrying capacity of the human population
s	Intrinsic growth rate of the human population
M	Carrying capacity of forest biomass
u	Intrinsic growth rate of forest biomass
θ	Human population decline coefficient due to CO_2 emissions
φ	Deforestation rate coefficient of forest biomass
π_1	Proportionality constant converting atmospheric CO_2 to forest biomass
π	Proportionality constant converting deforestation of forest biomass to human population

3. RESULTS

3.1. Existence, uniqueness, non-negativity, and boundedness of the solutions

Theorem 3.1. *Model (2) with initial value* $(X(0), N(0), F(0))$ *has a unique solution* $(X(t), N(t), F(t)) \in B$ *for all* $t \in [0,T], B = \{(X,N,F) \in \mathbb{R}^3 : \max\{|X|,|N|,|F|\} \leq \tau\}$.

Proof: We show existence and uniqueness of the solution of model (2) in region $B \times [0,T]$ where

$$B = \{(X,N,F) \in \mathbb{R}^3 : \max\{|X|,|N|,|F|\} \leq \tau\}.$$

Consider a mapping $\mathcal{H}(Z) = (\mathcal{H}_1(Z), \mathcal{H}_2(Z), \mathcal{H}_3(Z))$ where

$$\begin{aligned}
\mathcal{H}_1(Z) &= Q_0 + \lambda N - \alpha X - \lambda_1 XF, \\
\mathcal{H}_2(Z) &= sN\left(1 - \frac{N}{M}\right) - \theta XN + \pi_1\varphi NF, \\
\mathcal{H}_3(Z) &= uF\left(1 - \frac{F}{M}\right) - \varphi NF + \pi_1\lambda_1 XF.
\end{aligned}$$

For any $Z = (X,N,F)$, $\tilde{Z} = (\tilde{X},\tilde{N},\tilde{F})$, $Z, \tilde{Z} \in B$,

$$\|\mathcal{H}(Z) - \mathcal{H}(\tilde{Z})\| = \sum_{i=1}^{3} |\mathcal{H}_i(Z) - \mathcal{H}_i(\tilde{Z})|,$$

where

$$
\begin{aligned}
\|\mathcal{H}(Z)-\mathcal{H}(\tilde{Z})\| &= \left|Q_0+\lambda N-\alpha X-\lambda_1 XF-Q_0-\lambda\tilde{N}+\alpha\tilde{X}+\lambda_1\tilde{X}\tilde{F}\right| \\
&\quad+\left|sN\left(1-\frac{N}{M}\right)-\theta XN+\pi_1\varphi NF-s\tilde{N}\left(1-\frac{\tilde{N}}{M}\right)+\theta\tilde{X}\tilde{N}-\pi_1\varphi\tilde{N}\tilde{F}\right| \\
&\quad+\left|uF\left(1-\frac{F}{M}\right)-\varphi NF+\pi_1\lambda XF-u\tilde{F}\left(1-\frac{\tilde{F}}{M}\right)+\varphi\tilde{N}\tilde{F}-\pi_1\lambda\tilde{X}\tilde{F}\right|, \\
&= \left|\lambda(N-\tilde{N})-\alpha(X-\tilde{X})-\lambda_1 F(X-\tilde{X})-\lambda_1\tilde{X}(F-\tilde{F})\right| \\
&\quad+\left|s(N-\tilde{N})-\frac{s}{L}(N+\tilde{N})(N-\tilde{N})+\pi\varphi F(N-\tilde{N})\right. \\
&\qquad\left.+\pi\varphi\tilde{N}(F-\tilde{F})-\theta N(X-\tilde{X})-\theta\tilde{X}(N-\tilde{N})\right| \\
&\quad+\left|u(F-\tilde{F})-\frac{u}{M}(F-\tilde{F})(F+\tilde{F})-\varphi F(N-\tilde{N})-\varphi\tilde{N}(F-\tilde{F})\right. \\
&\qquad\left.+\pi_1\lambda_1 F(X-\tilde{X})+\pi_1\lambda_1\tilde{X}(F-\tilde{F})\right|, \\
&\le \alpha|X-\tilde{X}|+\lambda_1|F||X-\tilde{X}|+\theta|N||X-\tilde{X}|+\pi_1\lambda_1|F||X-\tilde{X}|+\lambda|N-\tilde{N}| \\
&\quad+s|N-\tilde{N}|+\frac{s}{L}|N+\tilde{N}||N-\tilde{N}|+\pi\varphi|F||N-\tilde{N}|+\theta\tilde{X}|N-\tilde{N}| \\
&\quad+\varphi|F||N-\tilde{N}|+\lambda_1\tilde{X}|F-\tilde{F}|+\pi\varphi\tilde{N}|F-\tilde{F}|+u|F-\tilde{F}| \\
&\quad+\frac{u}{M}|F+\tilde{F}||F-\tilde{F}|+\varphi\tilde{N}|F-\tilde{F}|+\pi_1\lambda_1\tilde{X}|F-\tilde{F}|.
\end{aligned}
\tag{4}
$$

By using the Lipschitz property and $\max(|X|,|N|,|F|)=\tau$, we have

$$\|\mathcal{H}(Z)-\mathcal{H}(\tilde{Z})\|\le\gamma\|Z-\tilde{Z}\|,$$

where $\gamma=\max(\gamma_1,\gamma_2,\gamma_3)$ and $\gamma_1=\alpha+\lambda_1\tau+\theta\tau+\pi_1\lambda_1\tau$, $\gamma_2=\lambda+s+\frac{s\tau}{L}+\pi\varphi\tau+\theta\bar{X}+\varphi\tau$, $\gamma_3=\lambda_1\bar{X}+\pi\varphi\bar{N}+u+\frac{u}{M}\tau+\varphi\bar{N}+\pi_1\lambda_1\bar{X}$. Thus, $\mathcal{H}(Z)$ satisfies the Lipschitz condition such that there is a unique solution $(X(t),N(t),F(t))\in B$ for all $t\in[0,T]$ with initial value $Z(0)=(X(0),N(0),F(0))$. ■

Theorem 3.2. *All solutions of model (2) for any initial value $(X(0),N(0),F(0))\in\mathbb{R}^3_+$ are always nonnegative.*

Proof: Suppose, $A(t_0)=(X(t_0),N(t_0),F(t_0))\in\mathbb{R}^3_+$ as the initial condition of the solution model (2). Let there exist a constant t_1 satisfying $0\le t\le t_1$ and

$$\begin{cases}N(t)>0, & 0<t<t_1,\\ N(t)=0, & t=t_1,\\ N(t)<0, & t>t_1.\end{cases}$$

From Equation (2), $D^qN(t)\big|_{N(t)=0}=0$. Thus, from Lemma 6 in [19], it implies that $N(t)\big|_{t=t_1}=0$, which contradicts $N(t)\big|_{t>0}<0$. Therefore, the statement $N(t)\ge0$ for all $t\in[0,\infty)$ is true.

Using the same approach, it can be shown that $F(t)\ge0$ for all $t>0$. Then, for $X(t)$, we can use a similar argument. Suppose that it is not true that $X(t)$ is nonnegative for $t\ge0$. There exists $t_2>0$ such that

$$\begin{cases}X(t)>0, & 0<t<t_2,\\ X(t)=0, & t=t_2,\\ X(t)<0, & t>t_2.\end{cases}$$

Since $D^q X(t)\big|_{X(t_2)=0} = Q_0 + \lambda N(t_2) > 0$, $X(t)$ is a nondecreasing function. Based on Lemma 6 in [19], this shows that $X(t_2) = 0$, which is a contradiction to $X(t)\big|_{t>t_2} < 0$. As a result, $X(t) \geq 0$ for all $t \in [0, \infty)$.

■

Theorem 3.3. *All solution of model (2) initiating from $W(0) = (X(0), N(0), F(0))$ remain bounded in the region B.*

Proof: Let us define a function, namely $W(t) = \pi\lambda\pi_1 X(t) + \lambda N(t) + \pi\lambda F(t)$. The Caputo derivative of q-order of $W(t)$ satisfies

$$\frac{d^q W}{dt^q} = \pi\lambda\pi_1 \frac{d^q X}{dt^q} + \lambda \frac{d^q N}{dt^q} + \pi\lambda \frac{d^q F}{dt^q},$$

where

$$\begin{aligned}\frac{d^q W}{dt^q} &= Q_0\pi\lambda\pi_1 + \pi\lambda\pi_1\lambda N - \pi\lambda\pi_1\alpha X - \pi\lambda\pi_1\lambda_1 XF + \lambda sN\left(1 - \frac{N}{L}\right) - \lambda\theta XN \\ &\quad + \lambda\pi\varphi NF + \pi\lambda uF\left(1 - \frac{F}{M}\right) - \pi\lambda\varphi NF + \pi\lambda\pi_1\lambda_1 XF, \\ &\leq Q_0\pi\lambda_1 + \lambda sL + \pi\lambda_1 M - \pi\lambda_1 aX - (s - \pi\lambda_1)\lambda N - u\pi\lambda F.\end{aligned}$$

Choose $\omega = \min\{a, s - \pi\lambda_1, u\}$ and $\delta = Q_0\pi\lambda_1 + \lambda sL + \pi\lambda_1 M$, then

$$\frac{d^q W}{dt^q} + \omega W \leq \delta.$$

Based on Lemma 3 in [20], we have

$$W(t) \leq \left(W_0 - \frac{\delta}{\omega}\right) E_q(-\omega t^q) + \frac{\delta}{\omega}. \tag{5}$$

Since $E_q(-\omega t^q) \to 0$ as $t \to \infty$, so that $W(t) \to \frac{\delta}{\omega}, \quad t \to \infty$. Therefore, we establish the following theorem. ■

3.2. Equilibria Analysis

The model (2) has the following equilibrium points.

1) The CO_2 concentration only equilibrium point $E_0\left(\frac{Q_0}{\alpha}, 0, 0\right)$.
2) The forest biomass-extinction equilibrium point $E_1(X_1, 0, F_1)$ where $X_1 = \frac{Q_0}{\alpha + \lambda_1 F_1}$ and $F_1 = \frac{1}{2\lambda_1}\left(M_1 - \alpha + \sqrt{(M_1 - \alpha)^2 + 4\lambda_1 M\left(\alpha + \frac{\pi_1\lambda_1 Q_0}{u}\right)}\right)$.
3) The coal mining-extinction equilibrium point $E_2 = (X_2, N_2, 0)$ with $X_2 = \frac{Q_0 + \lambda N_2}{\alpha}$ and $N_2 = \frac{L(\alpha s - \theta Q_0)}{\alpha s + \theta\lambda}$.
4) The coexistence equilibrium point $E^* = (X^*, F^*, N^*)$ where

$$X^* = \frac{Q_0 + \lambda N}{\alpha + \lambda_1 F^*} \quad \text{and} \quad N^* = \frac{\lambda_1 L\pi\varphi F^{*2} + (Ls\lambda_1 + \alpha L\pi\varphi)F^* + Ls\alpha - \theta LQ_0}{s\lambda_1 F^* + s\alpha + \theta L\lambda}.$$

F^* is obtained by solving the following cubic equation,

$$F^3 + 3\eta_1 F^2 + 3\eta_2 F + \eta_3 = 0, \tag{6}$$

with

$$\begin{aligned}
\eta_1 =& \frac{1}{3B_0}\left(\frac{\lambda_1 u(s\alpha+\theta L\lambda)}{M}+\varphi\lambda_1 L(s\lambda_1+\alpha\pi\varphi)-\lambda_1 L\pi\varphi(\pi_1\lambda_1\lambda-\varphi\alpha)-\frac{us\lambda_1}{M}(M\lambda_1-\alpha)\right),\\
\eta_2 =& \frac{1}{3B_0}\left(\varphi\lambda_1 L(s\alpha-\theta Q_0)-(\pi_1\lambda_1\lambda-\varphi\alpha)(Ls\lambda_1+\alpha L\pi\varphi)-aus\lambda_1\right.\\
&\left.-\frac{u(s\alpha+\theta L\lambda)(M\lambda_1-\alpha)}{M}-\pi_1 Q_0 s\lambda_1^2\right),\\
\eta_3 =& \frac{1}{B_0}\left(-(\pi_1\lambda_1\lambda-\varphi\alpha)(Ls\alpha-\theta LQ_0)-(\pi_1\lambda_1 Q_0+\alpha u)(s\alpha+\theta L\lambda)\right),\\
B_0 =& \lambda_1^2\left(\frac{us}{M}+\varphi^2 L\pi\right).
\end{aligned}$$

Through the transformation $\chi = F + \eta_1$, Equation (6) can be simplified to

$$g(\chi) = \chi^3 + 3p\chi + \kappa = 0, \tag{7}$$

where

$$p = \eta_2 - \eta_1^2, \quad \kappa = \eta_3 - 3\eta_1\eta_2 + 2\eta_1^3.$$

We can found roots of Equation (7) by using the Cardano's formula as follows [21],

$$\chi = \frac{\sqrt[3]{\left(-4\kappa \pm 4\sqrt{\kappa^2+4p^3}\right)^2} - 4p}{2\sqrt[3]{-4\kappa \pm 4\sqrt{\kappa^2+4p^3}}} \tag{8}$$

and we have $F^* = \chi - \eta_1$. Based on Lemma 3.1 from [22] the existence of positive roots for Equation (6) can be classified by the sign of κ and p:

- If $\kappa < 0$, there is exactly one positive root.
- If $\kappa > 0$ and $p < 0$:
  - $\kappa^2 + 4p^3 = 0$: one double positive root.
  - $\kappa^2 + 4p^3 < 0$: two distinct positive roots.
- If $\kappa = 0$ and $p < 0$, there is a unique positive root.

3.3. Local and Global Stability Analysis

The linearization technique can be used to analyze local stability around each equilibrium point. At any point (X, N, F), the Jacobian matrix J of model (2) is given by

$$J(X,N,F) = \begin{pmatrix} -\alpha-\lambda_1 F & \lambda & -\lambda_1 X \\ -\theta N & s\left(1-\frac{2N}{L}\right)-\theta X+\pi\varphi F & \pi\varphi N \\ \pi_1\lambda_1 F & -\varphi F & u\left(1-\frac{2F}{M}\right)-\varphi N+\pi_1\lambda_1 X \end{pmatrix}.$$

Theorem 3.4. *The equilibrium point $E_0\left(\frac{Q_0}{\alpha},0,0\right)$ of model (2) is always unstable.*

Proof: The eigenvalues of matrix at $E_0\left(\frac{Q_0}{\alpha},0,0\right)$ are $\zeta_1 = -\alpha$, $\zeta_2 = s - \frac{\theta Q_0}{\alpha}$, $\zeta_3 = u + \pi_1\lambda_1\frac{Q_0}{\alpha}$. See that $|\arg(\zeta_1)| = \pi > \frac{q\pi}{2}$, $|\arg(\zeta_2)| = \pi > \frac{q\pi}{2}$, and $|\arg(\zeta_3)| = 0 < \frac{q\pi}{2}$, Based on Matignon's condition, the equilibrium point E_0 is a saddle point. ■

We now analyze the stability of equilibrium point E_1. The Jacobian matrix of model (2) at E_1 is given by

$$J(E_1) = \begin{pmatrix} -\alpha-\lambda_1 F_1 & \lambda & -\lambda_1 X_1 \\ 0 & s-\theta X_1+\pi\varphi F_1 & 0 \\ \pi_1\lambda_1 F_1 & -\varphi F_1 & u\left(1-\frac{2F_1}{M}\right)+\pi_1\lambda_1 X_1 \end{pmatrix}.$$

Eigenvalues of matrix $J(E_1)$ are obtained by solving the characteristic equation

$$(\zeta^2 - \gamma_a\zeta + \gamma_b)\left(s - \frac{Q_0\theta}{\alpha + \lambda_1 F_1} + \pi\varphi F_1 - \zeta\right) = 0 \tag{9}$$

where

$$\begin{aligned}\gamma_a =& -\left(u - \frac{\pi_1\lambda_1 Q_0}{\alpha + \lambda_1 F_1} + \alpha + \left(\frac{2u}{M} + \lambda_1\right)F_1\right),\\ \gamma_b =& \lambda_1^2 X_1\pi_1 F_1 - (\alpha + \lambda_1 F_1)\left(\frac{u(M - 2F_1)}{M} + \frac{Q_0\pi_1\lambda_1}{\alpha + \lambda_1 F_1}\right).\end{aligned}$$

The roots of Equation (9) are $\zeta_1 = s - \frac{Q_0\theta}{\alpha+\lambda_1 F_1} + \pi\varphi F_1$ and

$$\zeta_{2,3} = \frac{1}{2}\left(\gamma_a \pm \sqrt{R_1}\right), \quad R_1 = \gamma_a^2 - 4\gamma_b.$$

By analyzing these eigenvalues, the stability of E_1 is stated in the following theorem.

Theorem 3.5. *The model (2) shows stable behaviour near the equilibrium point corresponding to human population extinction E_1 when $s + \pi\varphi F_1 < \frac{Q_0\theta}{\alpha+\lambda_1 F_1}$ and one of the following mutually exclusive conditions holds:*

1) $R_1 \geq 0$ *and* $\gamma_a < 0, \gamma_b > 0$,
2) $R_1 < 0, \gamma_a < 0$.
3) $R_1 < 0$, $\gamma_a = 0$, *and* $\gamma_b > 0$,
4) $R_1 < 0$, $\gamma_a > 0$, *and* $\frac{\sqrt{|R_1|}}{\gamma_a} > \tan\left(\frac{q\pi}{2}\right)$.

In a similar way, at the equilibrium point of forest biomass extinction, the Jacobian matrix J of model (2) is followed by

$$J(E_2) = \begin{pmatrix} -\alpha & \lambda & -\lambda_1 X_2 \\ -\theta N_2 & s\left(1 - \frac{2N_2}{L}\right) - \theta X_2 & \pi\varphi N_2 \\ 0 & 0 & u - \varphi N_2 + \pi_1\lambda_1 X_2 \end{pmatrix}.$$

It is easy to see that $\zeta = u - \varphi N_2 + \pi_1\lambda_1 X_2$ is an eigenvalue of the Jacobian matrix $J(E_2)$. The other eigenvalues of matrix $J(E_2)$ are obtained by solving the following equation

$$\zeta^2 - \zeta\gamma_c + \gamma_d = 0 \quad , \tag{10}$$

where $\gamma_c = -\alpha + s\left(1 - \frac{2N_2}{L}\right) - \theta X_2$ and $\gamma_d = \theta N_2\lambda - \alpha s\left(1 - \frac{2N_2}{L}\right) + \alpha\theta X_2$. Suppose that R_2 is the discriminant of (10) i.e., $R_2 = \gamma_c^2 - 4\gamma_d$. If $u + \pi_1\lambda_1 X_2 < \varphi N_2$ then $|\arg(\zeta_3)| > \frac{q\pi}{2}$. The stability of the equilibrium point of forest biomass extinction is determined through eigenvalue analysis given in the following theorem.

Theorem 3.6. *The model (2) shows stable behaviour near the equilibrium point of forest biomass extinction E_2 when $u + \pi_1\lambda_1 X_2 < \varphi N_2$ and one of the following mutually exclusive conditions holds:*

1) $R_2 \geq 0$ *and* $\gamma_c < 0, \gamma_d > 0$,
2) $R_2 < 0, \gamma_c < 0$,
3) $R_2 < 0$, $\gamma_c = 0$, *and* $\gamma_d > 0$,
4) $R_2 < 0$, $\gamma_c > 0$, *and* $\frac{\sqrt{|R_2|}}{\gamma_c} > \tan\left(\frac{\pi q}{2}\right)$.

We then analyzed the local asymptotic stability behavior at the interior equilibrium point. The Jacobian matrix of model (2) at E^* is presented by

$$J(X^*, N^*, F^*) = \begin{pmatrix} a_{11} & a_{12} & a_{13} \\ a_{21} & a_{22} & a_{23} \\ a_{31} & a_{32} & a_{33} \end{pmatrix},$$

where

$$a_{11} = -\alpha - \lambda_1 F^*, \quad a_{12} = \lambda, \quad a_{13} = -\lambda_1 X^*, a_{21} = -\theta N^*, \quad a_{22} = s\left(1 - \frac{2N^*}{L}\right) - \theta X^* + \pi\varphi F^*,$$

$$a_{23} = \pi\varphi N^*, \quad a_{31} = \pi_1\lambda_1 F^*, \quad a_{32} = -\varphi F^*, \quad a_{33} = u\left(1 - \frac{2F^*}{M}\right) - \varphi N^* + \pi_1\lambda_1 X^*.$$

The characteristic equation of the matrix $J(X^*, N^*, F^*)$ is

$$g(\zeta) = \zeta^3 + \gamma_e\zeta^2 + \zeta\gamma_f + \gamma_g = 0,$$

where

$$\gamma_e = -(a_{11} + a_{22} + a_{33}), \quad \gamma_f = -(a_{32}a_{23} + a_{31}a_{13} + a_{21}a_{12} - a_{33}a_{11} - a_{33}a_{22} - a_{11}a_{22})$$
$$\gamma_g = -(a_{11}a_{22}a_{33} + a_{12}a_{23}a_{31} + a_{13}a_{21}a_{32} - a_{21}a_{12}a_{33} - a_{31}a_{13}a_{22} - a_{32}a_{23}a_{11}).$$

Let $D(g)$ is the discriminant of $g(\zeta)$, it can be written as

$$D(g) = 18\gamma_e\gamma_f\gamma_g + (\gamma_e\gamma_f)^2 - 4\gamma_g\gamma_e^3 - 4\gamma_f^3 - 27\gamma_g^2. \tag{11}$$

Using Routh-Hurwitz stability criteria defined in Ahmed et al. [23], we obtained the following results.

Theorem 3.7. *The interior equilibrium point is stable if one of the following assumptions holds:*

1) $D(g) > 0$, $\gamma_e > 0$, $\gamma_e\gamma_f > \gamma_g$ *and* $\gamma_g > 0$.
2) $D(g) < 0$, $\gamma_e \geq 0$, $\gamma_f \geq 0$, $\gamma_g > 0$ *and* $q < \frac{2}{3}$.
3) $D(g) < 0$, $\gamma_e < 0$, $\gamma_f < 0$ *and* $q \geq \frac{2}{3}$.
4) $D(g) < 0$, $\gamma_e > 0$, $\gamma_f > 0$, $\gamma_e\gamma_f = \gamma_g$ *and* $q \in [0, 1]$.

In this section, we analyze the global asymptotic stability criterion of model (2) at the interior equilibrium point.

Theorem 3.8. *If* $X^* > \frac{\pi\lambda\pi_1}{\theta}$ *then the interior equilibrium point* E^* *of the model (2) is asymptotically stable globally.*

Proof: Since (X^*, N^*, F^*) is the interior equilibrium point of the model (2), we have

$$Q_0 + \lambda N^* - \alpha X^* - \lambda_1 X^* F^* = 0, \quad SN^*\left(1 - \frac{N^*}{L}\right) - \theta X^* N^* + \pi\varphi N^* F^* = 0,$$
$$\text{and} \quad uF^*\left(1 - \frac{F^*}{M}\right) - \varphi N^* F^* + \pi_1\lambda_1 X^* F^* = 0.$$

Consider the following positive definite Lyapunov function

$$V(X, N, F) = \frac{1}{2}(X - X^*)^2 + m_1\left(N - N^* - N^*\ln\frac{N}{N^*}\right) + m_2\left(F - F^* - F^*\ln\frac{F}{F^*}\right), \tag{12}$$

where m_1, m_2 are positive constants. Furthermore, the derivative of order q with respect to t of $V(X, N, F)$ along with the solution of model (2) is written as follows:

$$\begin{aligned}
\frac{d^qV}{dt^q} &\leq (X - X^*)(Q_0 + \lambda N - \alpha X - \lambda_1 XF) + m_1\left(\frac{N - N^*}{N}\right)\left(sN\left(1 - \frac{N}{L}\right) - \theta XN + \pi\varphi NF\right) \\
&\quad + m_2\left(\frac{F - F^*}{F}\right)\left(uF\left(1 - \frac{F}{M}\right) - \varphi NF + \pi_1\lambda_1 XF\right), \\
&= (X - X^*)(Q_0 + \lambda N - \alpha X - \lambda_1 XF) + m_1(N - N^*)\left(s\frac{N}{L} - \theta X + \pi\varphi F\right) \\
&\quad + m_2(F - F^*)\left(u\frac{F}{M} - \varphi N + \pi_1\lambda_1 X\right), \\
&= (m_2\pi_1 - X^*)\lambda_1(X - X^*)(F - F^*) + (\lambda - \theta m_1)(X - X^*)(N - N^*) \\
&\quad + \varphi(m_1\pi - m_2)(N - N^*)(F - F^*) - (\lambda_1 F + \alpha)(X - X^*)^2 - \frac{sm_1}{L}(N - N^*)^2 - \frac{um_2}{M}(F - F^*)^2,
\end{aligned}$$

Choose $m_1 = \frac{\lambda}{\theta}$ and $m_2 = \frac{\pi\lambda}{\theta}$, then

$$\frac{d^qV}{dt^q} = -\left(X^* - \frac{\pi\lambda\pi_1}{\theta}\right)\lambda_1(X-X^*)(F-F^*) - (\lambda_1 F+\alpha)(X-X^*)^2 - \frac{s\lambda}{L\theta}(N-N^*)^2 - \frac{u\pi\lambda}{M\theta}(F-F^*)^2 \tag{13}$$

Since $X^* > \frac{\pi\lambda\pi_1}{\theta}$ and $\max(|X|,|N|,|F|) \leq \tau$, we have

$$\frac{d^qV}{dt^q} \leq -\frac{\lambda_1}{2}\left(X^* - \frac{\pi\lambda\pi_1}{\theta}\right)\left((X-X^*)^2 + (F-F^*)^2\right) - (\lambda_1\tau+\alpha)F^*(X-X^*)^2 - \frac{s\lambda}{L\theta}(N-N^*)^2 - \frac{u\pi\lambda}{M\theta}(F-F^*)^2.$$

Clearly, $\frac{d^qV}{dt^q} \leq 0$ for all $(X,N,F) \in \mathbb{R}^3_+$ and $\frac{d^qV}{dt^q} = 0$ implies that $(X,N,F) = (X^*,N^*,F^*)$. Therefore, the only invariant set on which $\frac{d^qV}{dt^q} = 0$ is the singleton set $\{E^*\}$. By Lemma 4.6 [24], it is evident that the unique interior equilibrium point E^* is globally asymptotically stable if $X^* > \frac{\pi\lambda\pi_1}{\theta}$. This ends the proof of the Theorem.

■

3.4. Hopf Bifurcation Analysis

In this section, the Hopf bifurcation of model (2) is further examined using the stability theory of fractional-order systems, with a focus on selecting appropriate bifurcation parameters. Specifically, q and λ_1 are chosen as bifurcation parameters.

Theorem 3.9. *Suppose that* $\{A,B\} \in \mathbb{R}$ *and* $3(A+B) < \gamma_e < \sqrt{3\gamma_f}$. *Hopf bifurcation of the model (2) will appear around* E^* *when the fractional order* q *passes the critical value* $q^* = \frac{2}{\pi}\left|\arg(\zeta_{2,3})\right|$.

Proof: From the Jacobi matrix $J(E^*)$, the characteristic equation $\zeta^3 + \gamma_e\zeta^2 + \zeta\gamma_f + \gamma_g = 0$ is obtained. The eigenvalues are found by using Cardan's criteria [21, 25], namely $\zeta_1 = A + B - \frac{\gamma_e}{3}$ and $\zeta_{2,3} = \theta \pm \sigma i$ where

$$P = \gamma_f - \frac{\gamma_e^2}{3}, \quad Q = \frac{2\gamma_e^3}{27} - \frac{\gamma_e\gamma_f}{3} + \gamma_g, \quad \Delta = \left(\frac{Q}{2}\right)^2 + \left(\frac{P}{3}\right)^3,$$
$$A = \sqrt[3]{\frac{Q}{2} + \sqrt{\Delta}}, \quad B = \sqrt[3]{\frac{Q}{2} - \sqrt{\Delta}}, \quad \theta = \frac{(A+B)}{2} - \frac{\gamma_e}{3}, \quad \sigma = \frac{(A-B)\sqrt{3}}{2}$$

Given that $\{A,B\} \in \mathbb{R}$ and $3(A+B) < \gamma_e < \sqrt{3\gamma_f}$, it follows that $\zeta_1 < 0$. Furthermore, there exists a pair of complex eigenvalues $\zeta_{2,3} = \theta \pm \sigma i$ of $J(E^*)$ in model (2) with $\theta > 0$. Consequently, it can be determined that there exists a parameter such that

$$m(q^*) = 0 \quad \text{and} \quad \left.\frac{dm(q)}{dq}\right|_{q=q^*} = \frac{\pi}{2},$$

where $m(q) = \frac{q\pi}{2} - \min\left|\arg(\zeta_i)_{i=2,3}\right|$. By using the existence theorem of the Hopf bifurcation from [26], the equilibrium point E^* undergoes a bifurcation at $q = q^* = \frac{2}{\pi}\left|\arg(\zeta_{2,3})\right|$.

■

4. NUMERICAL SIMULATIONS AND DISCUSSIONS

In this section, numerical methods are employed to analyze the dynamic behavior of the model (2) and validate the analytical results obtained in the previous section. The predictor–corrector approach, specifically the fractional Adams-Bashforth-Moulton method, is used to solve fractional-order ordinary differential equations, as proposed in [27]. The parameter values are hypothetically selected without relying on real data, with some values adopted from previously published articles [8, 16, 17]. The simulations are conducted using the parameter values listed in Table 2.

Simulation 1 aims to demonstrate the temporal variations in CO_2 concentration, human population, and forest biomass for different values of φ. As shown in Figure 1, an increase in the deforestation rate (φ) results in a substantial increase in atmospheric CO_2 concentration, while human population growth decelerates, and forest biomass experiences a significant decline. At lower deforestation rates (0.0001), CO_2 levels increase

Table 2: Parameter values for variation of simulations.

Notation	Unit	Simulation 1 (Varying φ)	Simulation 2 (Memory effect)	Simulation 3 (Bifurcation)
$X(0)$	ppm	300	300	800
$F(0)$	ton	350	350	230
$N(0)$	person	800	800	150
Q_0	ppm month^{-1}	1	1	1
λ	ppm (month person)$^{-1}$	0.05	0.05	0.05
α	month^{-1}	0.003	0.003	0.003
λ_1	(ton month)$^{-1}$	0.0001	0.0001	0.0001
s	month^{-1}	0.01	0.01	0.01
L	person	1000	1000	1000
θ	(ppm month)$^{-1}$	0.00001	0.00001	0.00001
u	month^{-1}	0.2	0.2	0.2
M	ton	2000	2000	2000
π	person (ton)$^{-1}$	0.01	0.01	0.01
φ	(person month)$^{-1}$	-	0.0003	0.0008
π_1	ton (ppm)$^{-1}$	0.01	0.01	0.01
q	-	0.98	-	-

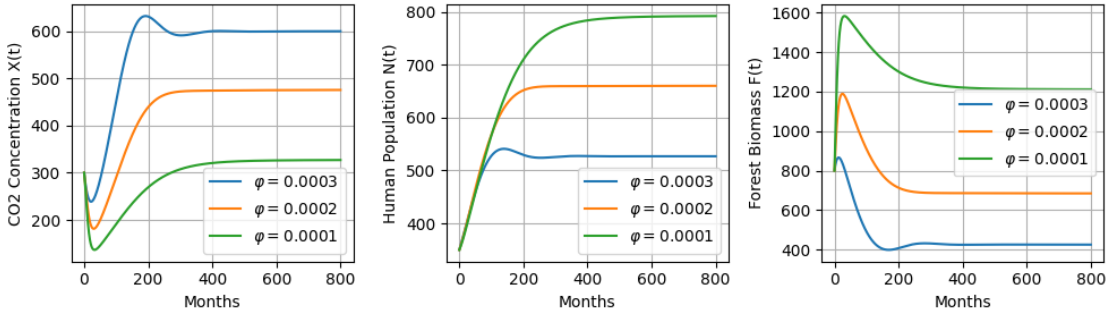

Figure 1: Time series of model (2) with $\varphi = 0.0001, 0.0002, 0.0003$.

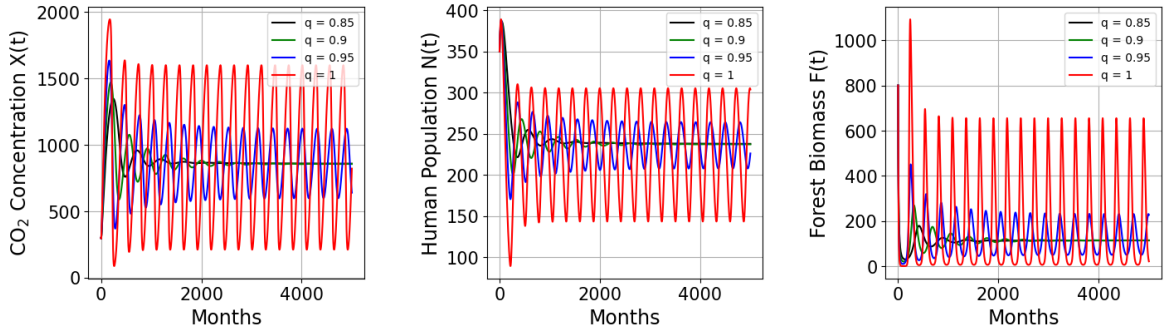

Figure 2: Time series of model (2) for varying order q.

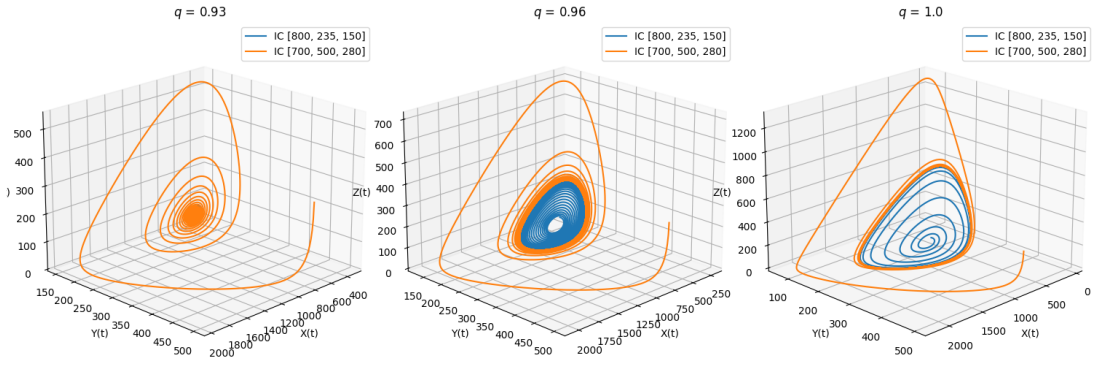

Figure 3: Phase portrait of model (2) for $q = 0.93, 0.96, 1$.

at a slower pace, allowing for more rapid human population growth and a higher retention of forest biomass. This figure underscores the detrimental effects of intensified deforestation on human populations.

In Simulations 2 and 3, we explore the role of memory in the dynamics of the fractional-order CO_2 model (2) considering the same parameter values as in Table 2. We consider the behavior of periodic solutions in the dynamics of the first-order model (1) and then observe the behavior of the dynamical system when the derived order q is continuously decreasing. Figure 2 depicts the first-order/classical model exhibiting periodic solutions for $q = 1$ (see red curve) and as the order of descent q decreases towards $q = 0.85$, the periodic oscillations of the model solutions decrease and eventually lead to a stable behavior with its periodic oscillations eliminated. Simulation 3 shows the phase portrait of a fractional order model with Hopf bifurcation affected by parameter q (see Figure 3). The critical point of bifurcation that occurs at $q = 0.9445$ can be seen in Figure 4. The Hopf bifurcation shows that the model remains stable for $0 < q < 0.9445$ and becomes unstable for $0.9445 \leq q \leq 1$. As the value of q increases, the model transitions from asymptotically stable oscillations to more centered and stable limit cycle orbits. This suggests that the long-term memory effect in fractional-order model contributes to improved stability and faster convergence to the equilibrium point. The bifurcation diagram with parameter λ_1 is shown in Figure 5 with parameter values as in Simulation 3 by replacing $q = 0.96$ and $0.001 \leq \lambda_1 \leq 0.009$. we have a bifurcation point at $\lambda_1^* = 0.0058$. For $\lambda_1^* \leq \lambda_1 \leq 0.09$, the solution converges to the co-existence point. The solution tends to the limit cycle in the range $0.001 \leq \lambda_1 < \lambda_1^*$.

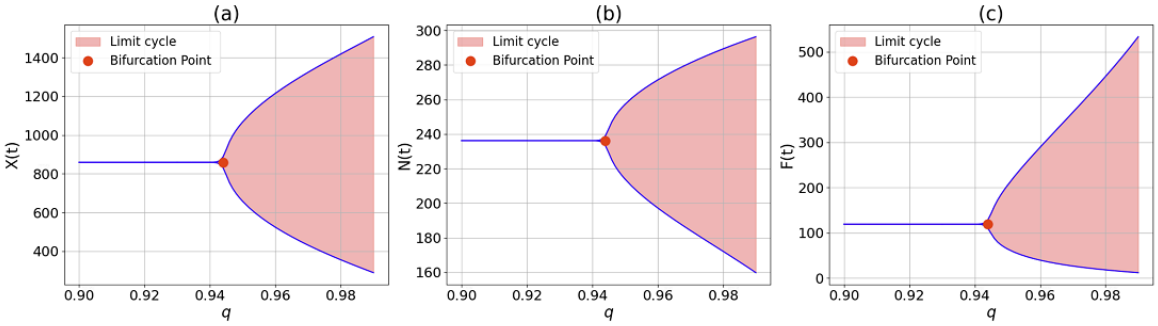

Figure 4: Bifurcation diagram of system (2) with respect to parameter q while the other parameter values are taken from Simulation 3 Table 2.

Numerical simulations of Caputo's fractional model show that the fractional derivative order q plays an important role in determining the dynamics of the CO_2-atmosphere, human population, and forest biomass

systems. For values of $q < 1$, the system exhibits a more stable and damped behavior, where oscillations in the three main variables (CO_2 concentration, human population and forest biomass) tend to subside over time and lead to a steady state. This reflects a significant memory effect on the model, where the response to change is gradual as the model 'remembers' previous conditions. In contrast, at $q = 1$, which represents the classical integer-order model, the system exhibits large amplitude and sustained oscillations, indicating more complex dynamics and potentially chaotic behavior.

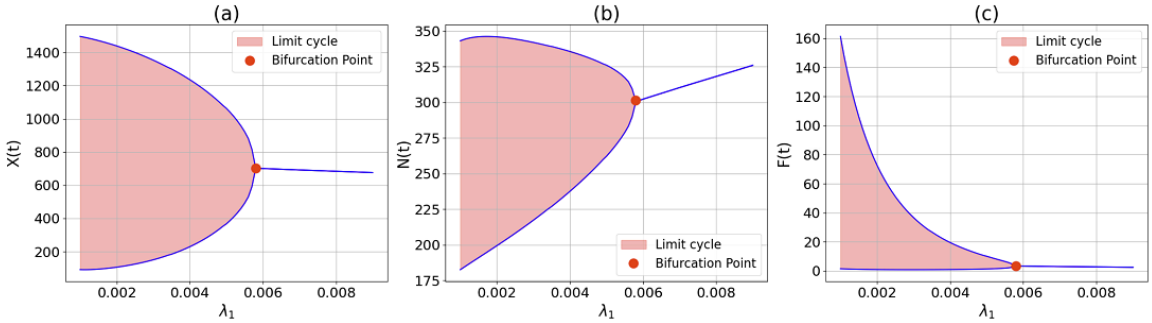

Figure 5: Bifurcation diagram of the model (2) with respect to parameter λ_1 for $q = 0.96$ and $0.001 \leq \lambda_1 \leq 0.009$.

Increasing rates of deforestation due to human activities significantly impact the dynamics of ecological and social systems. As anthropogenic parameters such as φ increase, forest biomass $F(t)$ decreases drastically due to reduced vegetation cover, which then triggers a spike in the concentration of CO_2 in the atmosphere $X(t)$ due to reduced carbon sinks. This has a direct impact on the human population $N(t)$, which shows a downward trend as environmental quality deteriorates. In contrast, under conditions where deforestation rates are low, forest ecosystems remain sustainable, CO_2 levels are more stable, and the human population can grow until it reaches long-term equilibrium. This phenomenon is supported by the results of the bifurcation analysis of the λ_1 parameter, shown in Figure 5. The diagram shows that if anthropogenic activity increases too quickly, a model that initially oscillates or fluctuates can become a stable state. In an ecological context, this means that environmental conditions can deteriorate dramatically, such as a significant reduction in forest biomass. Thus, these results emphasize that controlling the parameters φ and λ_1 is crucial as a strategic control point to reduce climate change and preserve the balance between ecological dynamics and social sustainability.

5. Conclusion

This study examines a Caputo-type fractional-order dynamical model for CO_2 concentration. Several sufficient conditions are investigated to ensure the existence, uniqueness, and boundedness of solutions, as well as the local and global stability of equilibrium points. Furthermore, the presence of Hopf bifurcation is explored in the fractional-order CO_2 concentration model. The findings indicate that stable asymptotic co-existence equilibrium points can occur both locally and globally under specific parameter conditions. Moreover, it is observed that when the derivative order parameter q exceeds a critical threshold, a Hopf bifurcation arises. The study further highlights the significant influence of fractional order on stability and the occurrence of Hopf bifurcation in the CO_2 concentration model. Finally, numerical simulations are performed to validate the theoretical findings, revealing that the Hopf bifurcation occurs at $q = 0.944$. To regulate CO_2 levels in the atmosphere, sustainable forest biomass management is essential to balance human population demands with environmental conservation. The insights gained from this study can contribute to maintaining the equilibrium between human activities and forest ecosystems.

Nevertheless, the proposed model has inherent limitations. It does not incorporate real-world data, and the parameter values used are hypothetical, which limits the model's predictive accuracy. Future research will face challenges in enhancing the model's validity by improving its capacity to reflect actual conditions . The integration of real-world data, such as accurate CO_2 concentrations, population dynamics, and forest biomass measurements, will be crucial to improving the model's reliability [28, 29]. Furthermore, the model does not

consider key factors such as reforestation, gross domestic product, and green technological innovation, all of which should be incorporated to provide a more comprehensive understanding of CO_2 dynamics and their socio-economic impacts [30]. Expanding the model to include these factors will help identify more targeted and effective policy recommendations. Additionally, the model could be enhanced by incorporating stochastic elements to better capture the unpredictability of real-world environmental changes.

ACKNOWLEDGMENTS

This research is funded by Faculty of Mathematics and Natural Science (FMIPA) through Public Funds DPA (Dokumen Pelaksanaan Anggaran) Perguruan Tinggi Negeri Berbadan Hukum (PTNBH), Brawijaya University and based on FMIPA Professor Grant, with contract number: 06871.19/N10.F0901/B/PT/2025, dated September 16, 2025.

REFERENCES

[1] NASA Global Climate Change, Carbon dioxide vital signs, 2023. https://climate.nasa.gov/vital-signs/carbon-dioxide/?intent=121, Accessed on February, 2025.
[2] Solomon, S., Plattner, G.-K., Knutti, R. and Friedlingstein, P., Irreversible climate change due to carbon dioxide emissions, Proceedings of the national academy of sciences, 106(6), pp. 1704–1709, 2009.
[3] Brovkin, V., Lorenz, S., Raddatz, T., Ilyina, T., Stemmler, I., Toohey, M. and Claussen, M., What was the source of the atmospheric CO2 increase during the holocene?, Biogeosciences, 16(13), pp. 2543–2555, 2019.
[4] Talukder, B., Loon, G.W. van, Hipel, K.W., Chiotha, S. and Orbinski, J., Health impacts of climate change on smallholder farmers, One Health, 13, p. 100258, 2021.
[5] Wu, X., Lu, Y., Zhou, S., Chen, L. and Xu, B., Impact of climate change on human infectious diseases: empirical evidence and human adaptation, Environment international, 86, pp. 14–23, 2016.
[6] Le Quéré, C., Andrew, R.M., Friedlingstein, P., Sitch, S., Hauck, J., Pongratz, J., Pickers, P.A., Korsbakken, J.I., Peters, G.P., Canadell, J.G., et al., Global carbon budget 2018, Earth System Science Data, 10(4), pp. 2141–2194, 2018.
[7] Baccini, A., Walker, W., Carvalho, L., Farina, M., Sulla-Menashe, D. and Houghton, R., Tropical forests are a net carbon source based on aboveground measurements of gain and loss, Science, 358(6360), pp. 230–234, 2017.
[8] Misra, A.K. and Verma, M., A mathematical model to study the dynamics of carbon dioxide gas in the atmosphere, Applied Mathematics and Computation, 219(16), pp. 8595–8609, 2013.
[9] Misra, A. and Jha, A., Modeling the role of renewable energy to mitigate the atmospheric level of carbon dioxide along with sustainable development, Chaos: An Interdisciplinary Journal of Nonlinear Science, 33(12), 2023.
[10] Misra, A. and Jha, A., How to combat atmospheric carbon dioxide along with development activities? a mathematical model, Physica D: Nonlinear Phenomena, 454, p. 133861, 2023.
[11] Tandon, A., Mathematical modelling and analysis to study the impact of mining on natural interactive dynamics between plants and carbon dioxide, Modeling Earth Systems and Environment, 9(1), pp. 97–110, 2023.
[12] Jha, A., Pal, S. and Misra, A., Impact of anthropogenic emissions of carbon dioxide and related temperature rise on wildlife population: a modeling study, Mathematics and Computers in Simulation, 223, pp. 229–252, 2024.
[13] Jha, A. and Misra, A., A robust role of carbon taxes towards alleviating carbon dioxide: a modeling study, Journal of Engineering Mathematics, 144(1), p. 20, 2024.
[14] Kumar, P. and Erturk, V.S., A variable-order fractional mathematical model for the strategy to combat the atmospheric level of carbon dioxide, Modeling Earth Systems and Environment, pp. 1–17, 2024.
[15] Ilhan, E., Veeresha, P. and Baskonus, H.M., Fractional approach for a mathematical model of atmospheric dynamics of CO2 gas with an efficient method, Chaos, Solitons & Fractals, 152, p. 111347, 2021.
[16] Dubey, V.P., Dubey, S., Kumar, D. and Singh, J., A computational study of fractional model of atmospheric dynamics of carbon dioxide gas, Chaos, Solitons & Fractals, 142, p. 110375, 2021.
[17] Singh, J., Agrawal, R. and Nisar, K.S., A new forecasting behavior of fractional model of atmospheric dynamics of carbon dioxide gas, Partial Differential Equations in Applied Mathematics, 9, p. 100595, 2024.
[18] Petráš, I., Fractional-order nonlinear systems: modeling, analysis and simulation, Springer Science & Business Media, 2011.
[19] Boukhouima, A., Hattaf, K. and Yousfi, N., Dynamics of a fractional order hiv infection model with specific functional response and cure rate, International Journal of Differential Equations, 2017(1), p. 8372140, 2017.
[20] Li, H.-L., Zhang, L., Hu, C., Jiang, Y.-L. and Teng, Z., Dynamical analysis of a fractional-order predator-prey model incorporating a prey refuge, Journal of Applied Mathematics and Computing, 54, pp. 435–449, 2017.

[21] Wituła, R. and Słota, D., Cardano's formula, square roots, chebyshev polynomials and radicals, Journal of Mathematical Analysis and Applications, 363(2), pp. 639–647, 2010.
[22] Cai, Y., Zhao, C., Wang, W. and Wang, J., Dynamics of a leslie–gower predator–prey model with additive allee effect, Applied Mathematical Modelling, 39(7), pp. 2092–2106, 2015.
[23] Ahmed, E., El-Sayed, A. and El-Saka, H.A., On some Routh–Hurwitz conditions for fractional order differential equations and their applications in Lorenz, Rössler, Chua and Chen systems, Physics Letters A, 358(1), pp. 1–4, 2006.
[24] Huo, J., Zhao, H. and Zhu, L., The effect of vaccines on backward bifurcation in a fractional order HIV model, Nonlinear Analysis: Real World Applications, 26, pp. 289–305, 2015.
[25] Panigoro, H.S., Suryanto, A., Kusumawinahyu, W.M. and Darti, I., Dynamics of a fractional-order predator-prey model with infectious diseases in prey, Commun. Biomath. Sci, 2(2), pp. 105–117, 2019.
[26] Li, X. and Wu, R., Hopf bifurcation analysis of a new commensurate fractional-order hyperchaotic system, Nonlinear Dynamics, 78, pp. 279–288, 2014.
[27] Diethelm, K., Ford, N.J. and Freed, A.D., A predictor-corrector approach for the numerical solution of fractional differential equations, Nonlinear Dynamics, 29, pp. 3–22, 2002.
[28] Donald, P., Mayengo, M. and Lambura, A.G., Mathematical modeling of vehicle carbon dioxide emissions, Heliyon, 10(2), 2024.
[29] Fatmawati, F., Herdicho, F.F., Fitriani, N., Alias, N., Hashim, M. and Peter, O.J., Optimal control strategies for dynamical model of climate change under real data, Journal of the Nigerian Society of Physical Sciences, pp. 2572–2572, 2025.
[30] Begum, R.A., Raihan, A. and Said, M.N.M., Dynamic impacts of economic growth and forested area on carbon dioxide emissions in malaysia, Sustainability, 12(22), p. 9375, 2020.
[31] Odibat, Z.M. and Shawagfeh, N.T., Generalized taylor's formula, Applied Mathematics and Computation, 186(1), pp. 286–293, 2007.